Geomechanics and Engineering, *Vol. 27, No. 5 (2021) 465-479*
https://doi.org/10.12989/gae.2021.27.5.465

Numerical FEM assessment of soil-pile system in liquefiable soil under earthquake loading including soil-pile interaction

Mehdi Ebadi-Jamkhaneh[1a], Amir Homaioon-Ebrahimi[2b], Denise-Penelope N. Kontoni*[3,4] and Maedeh Shokri-Amiri[5c]

[1]*Department of Civil Engineering, School of Engineering, Damghan University, Damghan, Iran*
[2]*Department of Civil Engineering, School of Engineering, University of Birmingham, Birmingham, UK*
[3]*Department of Civil Engineering, School of Engineering, University of the Peloponnese, GR-26334 Patras, Greece*
[4]*School of Science and Technology, Hellenic Open University, GR-26335 Patras, Greece*
[5]*School of Literature, Humanities and Social Sciences, Science and Research Branch, Islamic Azad University, Tehran, Iran*

(Received May 28, 2021, Revised August 14, 2021, Accepted November 10, 2021)

Abstract. One of the important causes of building and infrastructure failure, such as bridges on pile foundations, is the placement of the piles in liquefiable soil that can become unstable under seismic loads. Therefore, the overarching aim of this study is to investigate the seismic behavior of a soil-pile system in liquefiable soil using three-dimensional numerical FEM analysis, including soil-pile interaction. Effective parameters on concrete pile response, involving the pile diameter, pile length, soil type, and base acceleration, were considered in the framework of finite element non-linear dynamic analysis. The constitutive model of soil was considered as elasto-plastic kinematic-isotropic hardening. First, the finite element model was verified by comparing the variations on the pile response with the measured data from the centrifuge tests, and there was a strong agreement between the numerical and experimental results. Totally 64 non-linear time-history analyses were conducted, and the responses were investigated in terms of the lateral displacement of the pile, the effect of the base acceleration in the pile behavior, the bending moment distribution in the pile body, and the pore pressure. The numerical analysis results demonstrated that the relationship between the pile lateral displacement and the maximum base acceleration is non-linear. Furthermore, increasing the pile diameter results in an increase in the passive pressure of the soil. Also, piles with small and big diameters are subjected to yielding under bending and shear states, respectively. It is concluded that an effective stress-based ground response analysis should be conducted when there is a liquefaction condition in order to determine the maximum bending moment and shear force generated within the pile.

Keywords: earthquake loading; FEM; liquefaction; numerical modeling; pile; reinforced concrete; soil-pile interaction

1. Introduction

Regardless of the results of the progressive accumulation of pore water pressures in the saturated soil, the performance of piles in liquefiable soil under earthquake loading is a complex issue. Due to liquefaction, the loss of soil strength and stiffness can result in broad bending moments and shear forces in piles formed in liquefiable soil, resulting in pile damage. The severity of liquefaction-related disruption to pile foundations was illustrated by the major earthquakes that have occurred over the last few years.

The mechanisms involved in pile-soil-structure interaction (PSSI) in liquefiable soil are several ambiguities, although the data provided during the earthquakes, shake table tests (Ohtomo 1996, Tamura *et al*. 2000, Yasuda *et al*. 2000, Mizuno *et al*. 2000, Nakamura *et al*. 2000), and centrifuge tests (Dobry *et al*. 1995, Abdoun *et al*. 1997, Horikoshi *et al*. 1998, Wilson *et al*. 1999, 2000) provide insight into the mechanism of PSSI in liquefiable soil.

Different approaches such as centrifuge and shaking table tests as well as numerical models were suggested to analyze the dynamic response of the single pile and group of piles. The PSSI was studied using centrifuge tests (Gohl and Finn 1987, Chang and Kutter 1989, Liu and Dobry 1995, Hushmand *et al*. 1998, Wilson 1998, Abdoun and Dobry 2002, Su and Li 2006) and shaking table test (Mizuno and Liba 1982, Yao *et al*. 2004, Tamura and Tokimatsu 2005, Han *et al*. 2007, Gao *et al*. 2011, Zhang *et al*. 2020, Haeri *et al*. 2012, Ebeido *et al*. 2019). The evident advantage of shaking table and centrifuge tests includes measurability of response in a series of tests designed for quake important features physical assessment (e.g., excitation level and frequency content), soil profile and pile, and superstructure specifications (Wilson 1998). However, there are certain limitations in centrifuge tests, such as sand grains in centrifuge tests that were larger than the particles in a real sample (Towhata 2008).

*Corresponding author, Associate Professor
E-mail: kontoni@uop.gr
[a] Assistant Professor
E-mail: m.ebadi@du.ac.ir
[b] Ph.D.
E-mail: AXH552@alumni.bham.ac.uk
c M.Sc.
E-mail: maedeh.shokri@hotmail.com

ISSN: 2005-307X (Print), 2092-6219 (Online)

The long-term settlement characteristics for the cast-in-place bored pile in the deep-thick soft soil are investigated by post-grouting field tests (Zou *et al*. 2019). Watcharasawe *et al*. (2021) investigated the load sharing of the pile foundation during the construction of a high-rise building. They monitored axial forces in several piles, pore water pressure, and earth pressures beneath the raft in a tributary area through the construction period of the building. Finn and Fujita (2002), Tajirian *et al*. (2019), Zhang *et al*. (2018), Bagheri *et al*. (2018), Kheradi *et al*. (2019), Klar *et al*. (2004), Oka *et al*. (2004), Uzuoka *et al*. (2007), Cheng and Jeremic (2009), Comodromos *et al*. (2009), Rahmani and Pak (2012), Kim and Choi (2017), Jiang *et al*. (2018), Cui *et al*. (2018), and Chong *et al*. (2019) used finite element (FE) three-dimensional (3D) simulation approach to simulate piles in different soil layers. Complexity and time-consuming 3D non-linear FE approach for dynamic analyzing causes the same to be possible for quite major practical projects. However, the boundary conditions and releasing the same in the full 3D analysis may be used to attain a reasonable solution for pile non-linear response using more limited calculations. Hussein and El Naggar (2021) investigated the axial load transfer during seismic events for pile groups installed in loose and dense sand layers. The results of the liquefiable test demonstrated that the excess pore water pressure and associated liquefaction during the shaking caused a dramatic decrease in the shaft friction resistance. Jiménez et al. (2019) investigated the effects of the liquefaction phenomenon on a 3-storey reinforced concrete building founded on pile systems. Their results revealed that maximum bending moments are located at the intersection with the liquefiable soil.

Khakpour Moghaddam *et al*. (2015) investigated the underground water level effects on the nonlinear behavior of a single pile subjected to static vertical loads in the presence of soil-pile interaction. Bahrami *et al*. (2015) investigated numerically and parametrically the dynamic soil-pile interaction during the passage of Rayleigh waves using Fourier transform. Kontoni and Farghaly (2018) studied a riverine platform together with its pile group foundation under environmental loads (water current and wave loads, wind loads) and static loads using 3D FEM structural analysis incorporating soil-pile interaction. Farghaly and Kontoni (2018) performed materially nonlinear earthquake response spectrum analyses on the 3D FEM models of a riverine platform supported by piles under earthquake and environmental loads considering soil-pile interaction.

In this study, a FEM numerical model has been suggested for the simulation of pile behavior in liquefiable soil under seismic earthquake loading, including soil-pile interaction. The main variables in this study include pile diameter and length, soil type, and earthquake peak gravity acceleration. The innovation of this study is that liquefiable soil model behavior was implemented in the ABAQUS software, considering in the analysis different layers of sandy soil with two layers of liquefiable soils in different levels. Non-linear dynamic analyses are conducted considering non-linear mechanical and geometrical specifications and soil-pile interaction. The numerical results obtained by the finite element method are first verified using centrifuge test results, and then the effect of different parameters on the pile behavior is investigated.

2. Numerical modeling

2.1 Elements specifications

In this study, a set of 3D non-linear analyses was conducted by taking benefit from ABAQUS/Explicit software. The pile embedded in soil was modeled using non-linear beam element, and also pile mass was considered. To consider the pile-soil model stiffness, 8-node linear brick elements around the pile element were considered, whilst to do so, the pile 3D geometry is modeled realistically. In a 3D state, the nodes have six degrees of freedom, while the B32 and C3D8R types of elements have been used for pile and soil elements, respectively. B is referred to as beam-type element, 3 is referred to three dimensions, and 2 indicates that geometrical shape function is of second order. Foundation and soil elements are continuous elements subject to stress-strain analysis. Measurement of 8 indicates eight nodes, and R means reduced integration. Beam element center nodes are connected to the same height rigidly with their surrounding soil elements nodes. Therefore, each part of the pile acts as a rigid disc. On the other hand, rotation is free for each part, whilst the relevant plane remains perpendicular to the pile axis; however, elongation does not occur along with the element. Meanwhile, the soil is modeled with 8-node 3D continuous elements. Regarding this study, infinite elements have been used to remove the returning of quake waves and the generation of absorption boundaries in remote borders. Infinite elements (CIN3D8), through the effect of a damping matrix, include “quiet” boundaries to the FE model (Fig. 1).

The infinite elements introduce excessive normal and shear tractions on the FE boundary during dynamic steps in a way which are proportional to both velocities of the

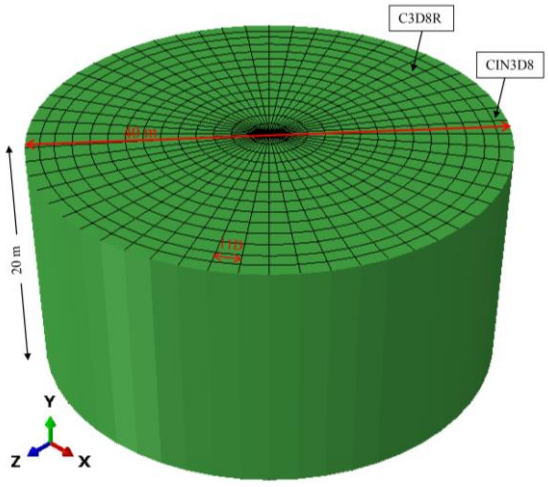

Fig. 1 Position of special elements in the finite element model

boundary normal and shear components. Such boundary damping constants are carefully selected in a certain manner to keep the reflection of dilatational and shear wave energies back into the FE mesh as low as possible. This method does not have a complete transfer of energy from the mesh, even in the case of plane body waves orthogonally impinging on the boundary in the isotropic medium. On the other hand, such a matter normally offers acceptable modeling regarding most of the relevant practical cases.

2.2 Materials behavior models

Two concrete and soil materials were applied in this model. The behavior model offered by Abate *et al*. (2008) has been applied for soil behavior modeling purposes. Such modeling is formulated based on kinematic bounding and hardening of surface plasticity, which may explain the general multiaxial stress-strain behavior of any granular materials concerning a wide range of both mean pressures and densities.

The executed model merges the following: the critical state, the dependence of strength, stiffness on the state parameter ψ, and finally Drucker-Prager yielding, all offered by Been and Jefferies (1985), as a non-associated flow role derived from that of the Cam-Clay model as well as a hyperbolic law for plastic stiffness degradation. It has three surfaces as follows: the strength surface, the yield surface, and finally, the critical state surface. There surely is the problem of softening, which is prevented through formulating the elasto-plastic relations under "normalized" stress space, in which both the yield and strength surfaces are subject to a constant size, while the ratio between the surface size of the yield and the surface size of the resistance is regarded a constitutive factor. It is to say that the aforementioned model enjoys having such a great advantage of being based on merely ten parameters as follows: eight plastic (k_d, B, k, R, ν_λ, λ, ϕ_{cv}, A) and two elastic (E and n) all to be determined using simple tri-axial testing.

In the meantime, especially ν_λ and λ can define the local point of the critical-state line, while B defines the hyperbolic plastic stiffness relationship, ϕ_{cv} defines the critical-state strength, k and R define the yield and strength surfaces, and finally, A and k_d define the flow rule. The foregoing model has been executed by the authors of this article using the ABAQUS software. The strength and stiffness of the soil depend on the state parameter ψ defined by:

$$\psi = \nu - \nu_\lambda + \lambda \ln p \tag{1}$$

The specific volume is shown with ν, and the average effective pressure is represented by p. are There are two constitutive parameters which are defined by ν_λ and λ The strength and the critical state surface are linked by Eq. 2. In this relation, k is defined as a constitutive factor.

$$r = 1 - k\psi \tag{2}$$

where ψ is the state parameter.

The failure and resistance surfaces for cohesionless soil are represented by the Drucker-Prager surface:

$$F = \alpha^* I + \sqrt{J} \tag{3}$$

where

$$\alpha^* = \frac{2\sin\varphi}{\sqrt{3}(3-\sin\varphi)} \tag{4}$$

and φ is the friction angle of the soil. Ultimately, a non-associative flow law is described. In particular, there is no clear description of the potential function. However, the direction tensor of plastic increment strain m with a unit standard is defined as follows:

$$m = \frac{\bar{m}}{\sqrt{\bar{m}:\bar{m}}} \tag{5}$$

where

$$\bar{m} = \frac{\sqrt{3}}{2\sqrt{J_\mu}}\mu - \frac{d}{\sqrt{3}}\delta \tag{6}$$

and

$$J_\mu = \frac{1}{2}\mu:\mu \tag{7}$$

$$\mu = n - (n:\delta)\delta \tag{8}$$

$$n = \left(\frac{\partial f}{\partial \bar{\sigma}}\right) \Big/ \left(\sqrt{\frac{\partial f}{\partial \bar{\sigma}}:\frac{\partial f}{\partial \bar{\sigma}}}\right) \tag{9}$$

$$d = \frac{\delta\varepsilon_v^p}{\delta\varepsilon_s^p} = -A[(1 + k_d\psi)G(\varphi_{cv}) - G(\varphi_m)] \tag{10}$$

In Eqs. 7-10, considering original Cam Clay formulation, δ is the unit norm tensor referring to the principal stress space bisector of the first quadrant, d is the dilatancy, n is the unit standard direction tensor that distinguishes between loading and unloading, k_d and A are two soil constitutive factors, and G(φ) is an arbitrary function as shown in Eq. 11.

$$G(\varphi) = (6\sin\varphi)/(3-\sin\varphi) \tag{11}$$

It is worth mentioning that φ_m is considered as an equivalent current mobilized friction angle, which highly depends on the relevant strength surface chosen shape. Hence, we also have the following formula:

$$\delta\varepsilon^p = \frac{B\beta_{max}}{\beta^2(n:\delta\bar{\sigma})} \tag{12}$$

where B is a constitutive parameter, $\beta = n:(\bar{\sigma}_c - \bar{\sigma})$, $\beta(1-R)\left(\hat{\bar{\sigma}}_c - \bar{\sigma}\right)_{max}$, and $\bar{\sigma}_c$ is the stress state. Upon flow rule definition, merely the deviatoric component of "m" should coincide with the deviatoric component of "n". Finally, the fact is that the incremental link between total strain ε and total stress $\bar{\sigma}$ in the normalized stress space may be given as per the following:

$$\delta\bar{\sigma} = \left[\bar{D}^e - \frac{(\bar{D}^e:m^*)\otimes(n:\bar{D}^e)}{H + n:(\bar{D}^e:m^*)}\right]:\delta\varepsilon \tag{13}$$

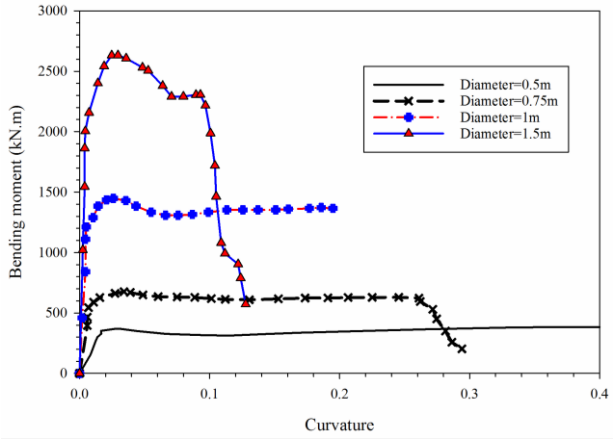

Fig. 2 Bending moment-curvature curves for reinforced concrete piles

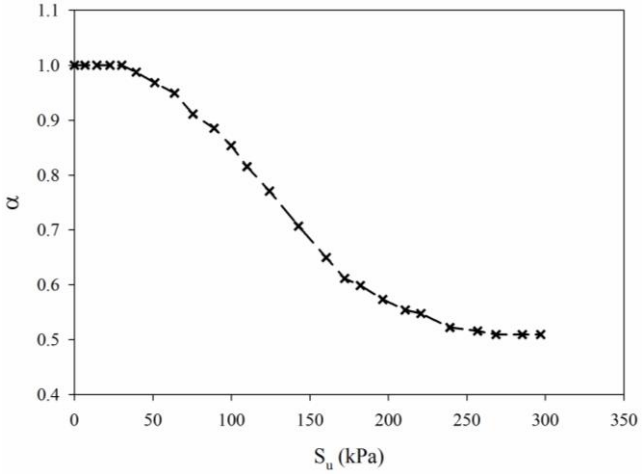

Fig. 3 Relationship between friction coefficient and contact pressure in the boundary between soil and pile

where m* is the change in m (Eq. 5) on moving from the 'true' to the normalized stress space, $\bar{D}^e$ is the elastic stiffness matrix in the normalized stress space, considering assuming a soil isotropic elastic behavior, $H = \beta^2/B\beta_{max}$, and n is the tensor with unit norm defined in Eq. 9.

The foregoing code is able to conduct a significant number of static and dynamic numerical FEM analyses. As for the geotechnical constitutive models, the relevant user may select out of the following materials: elastic-perfectly plastic Mohr-Coulomb material, elastic-perfectly plastic Drucker-Prager material modified to include an elliptical cap hardening, linear elastic material, and Cam Clay material. These models are usually seen in many commercial codes. However, all fail to include, for instance, simultaneously the effects of density and average pressure and kinematic hardening, which are mainly quite significant for the study of granular materials studies, especially in terms of dynamic loading. Nevertheless, the aforementioned code enables the user to launch other material constitutive models by taking benefit from the User Material Model command.

Reinforced concrete piles are calculated based on the capacity for a single pile, and their non-linear behavior is compared with the proper moment-curvature relationship. A moment-curvature relationship may be calculated for section static analysis easily using certain software such as SAP2000 and Xtract. Fig. 2 shows the moment-curvature curve for piles of 0.5, 0.75, 1, and 1.5 m diameters. Concrete compressive strength is equal to 21 MPa, while longitudinal rebars have been used with 400 MPa yield stress. The number of longitudinal rebars in such piles is 12, 12, 18, and 18, respectively.

2.3 Mesh sizes

Trochanis *et al*. (1991) found out through examining different mesh sizes and placing the same beneath the mesh in the distance between 0.6 and 0.7 times of the buried length of the pile below the pile, good accuracy for pile FE simulation has been achieved. For instance, for a pile of 2 m diameter and length of 14 m, the size of the element shall be at least between 20 m and 23.5 m, and a diameter of 17 m. The effect of mesh diameter was studied using 10 diameters of 1D, 2D, 3D, 4D, 5D, 6D, 9D, 11D, 13D, and 15D. After a lot of simulations with different dimensions of the soil and especially the radius of the near- and far-field region, an accurate response was obtained for the pile with a far-field radius of 11D and a near-field radius of 5D. The number of total points and elements for each mesh was kept fixed. Considering the preceding, the studied 3D model includes 6133 elements and 9460 nodes, out of which 20 second-order B32 elements, and 5345 C3D8 elements for soil, and 768 CIN3D8 elements for soils have been used.

2.4 Soil-pile interaction

A contact is defined between soil and concrete pile with considering frictional behavior. Such contact enables real simulation of a slippery detachment of pile and soil contact interface. The rigid boundary in the lower part was considered for the base on a depth of 20 m. The response of two systems under dynamic loading is calculated by considering soil and pile non-linear behavior (uplift of the pile and the effects of geometry shape). The relationship between the peak friction coefficient α and the undrained shear strength (S_u) is depicted in Fig. 3 (Peck *et al*. 1974).

2.5 Method to apply soil initial effective conditions

Gravity loads are used for each simulation before applying an earthquake load to the pile. This case does not affect the load-settlement curves, while it gives a better demonstration of relative displacement (and shear stress distribution) between pile and soil. Fig. 4 shows the concept for stage simulation of soil initial effective stress. At pile location, two sets of elements have been defined. These sets have overlapping and joint nodes. A set of elements has the features of soil (soil column) with the weight beneath the ground surface and without its weight above ground level. Another set of elements is the concrete features (concrete column as pile). For initial conditions, elements are activated for the soil column, while the elements have been inactivated for the concrete pile. In the first stage, gravity loads are applied to the system. The remaining stresses are

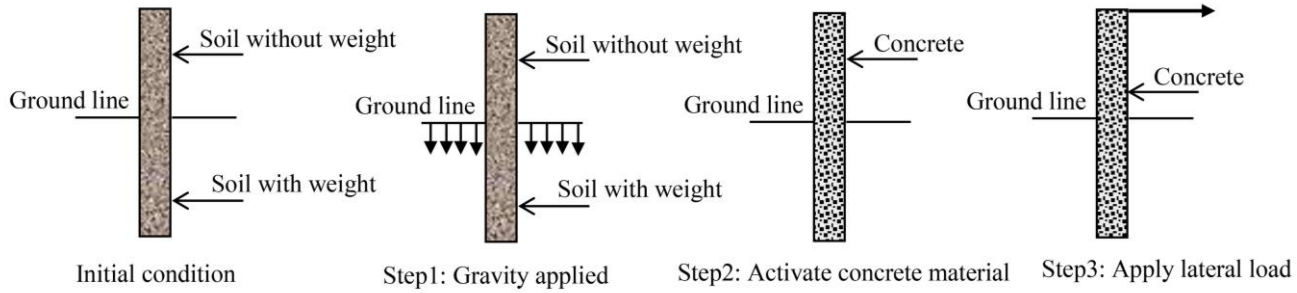

Fig. 4 Stages of applied effective stress on the soil

generated inside the soil, and the soil is settled. In the second stage, the soil column is inactivated, and the concrete pile is activated. Further settlement of this column area occurs because the concrete is heavier than the soil. Then in the third stage, the earthquake load is applied to the system.

2.6 Method to apply liquefaction conditions for sand soil layers

The most important factor in liquefaction is that there is a need for yield repetition modeling, accompanied by reduced shear stiffness and the development of liquefaction. As the shear module depends on effective stress, a decrease in stiffness may be resulted in the following equations through replacing G_{max} and τ_{max}.

$$\tau \frac{1}{2D_0}\int_{r_0}^{5r_0}\frac{(\sigma_r'-\sigma_\theta')}{2}_{max} \tag{14}$$

where σ_r' and σ_θ' are radial and tangential stresses in soil elements.

$$G_{max,u} = G\sqrt{(1-r_u)}_{max} \tag{15}$$

$$\tau_{max,u} = \tau(1-0.99r_u)_{max} \tag{16}$$

r_u is the pore-pressure water.

2.7 Specifications of earthquake and dimensions of pile and soil elements

In FE models, concrete 28-day cylindrical sample compressive strength has been considered as 21 MPa with the Poisson ratio as 0.2. It shall also be mentioned that the groundwater level is at a distance of 2 m from the ground level. In this study, piles with the length of 13 m and 16 m, with a variety of diameters (0.5 m, 0.75 m, 1 m, and 1.5 m), in the non-linear dynamic analysis under Kobe earthquake with four base accelerations of 0.05g, 0.1g, 0.15g, and 0.2g. This quake is the type of near-fault with 256 m/s shear wave velocity. Two liquefiable soil layers in two 5 m to 6 m and 11 m to 12 m depths were considered. Meanwhile, two sand soil layers of 7 m and 13 m thicknesses, internal friction angle of 28 and 38 degrees, and cohesion stress of 21 and 38 MPa are used. On the other hand, soil depth is 20 m, and its diameter is 40 m.

Table 1 Material properties for Nevada sand

Property	D_r=55%	D_r=80%
Mass density (kg/m^3)	2670	2670
Porosity	0.406	0.373
Low-strain shear modulus (MPa)	28	41.46
Reference effective normal stress (kPa)	100	100
Friction angle	34.15°	39.5°
Permeability (m/s)	6.05×10^{-5}	3.7×10^{-5}

3. Comparison with centrifuge data

Wilson *et al*. (1999) have compared centrifuge tests and have shown that the method can simulate pile behavior in the liquefaction of soil. In the centrifuge test that Wilson *et al*. (1999) conducted, two horizontal layers of Nevada sand that were saturated, fine, and uniformly graded composed the soil profile. The relative density (D_r) of the lower layer, which was dense and had a thickness of 11.4 m, was 80%, while that of the upper layer, which was medium dense with a thickness of 9.1 m, was 55%. The structural model was composed of a one-pile supported structure, equivalent to a steel pile of 0.67 m in diameter a 19 mm-thick wall. The pile went 3.8 m above the level of the ground surface, carrying a superstructure load equal to 480 kN. The embedment of the pile was approximately 15 m in depth. Table 1 shows the characteristics of Nevada sand (D_r=55%, 80%).

In Fig. 5 the acceleration record of the Kobe earthquake scaled to 0.22g generated for the centrifuge test by Wilson *et al*. (1999) and the comparison of the results of the FE model with the centrifuge test are shown. The model was analyzed with the acceleration record, which was scaled to 0.22 g in Fig. 5(a), like the earthquake in Kobe, but the frequency content had been slightly modified. In Fig. 5, we can see the pore pressure distribution, both measured and calculated, near the soil deposit surface, the acceleration of the superstructure, and the bending moment at a depth of 2.3 m. The distribution of the pore pressure recorded here demonstrates drastic declines because of the dilation of the soil. In the superstructure acceleration record, sharp spikes can be seen in the acceleration, which corresponds to the sharp declines in the pore pressure. This shows that the decrease in the pore pressure because of the dilation of the soil has raised the shear modulus of the soil. The

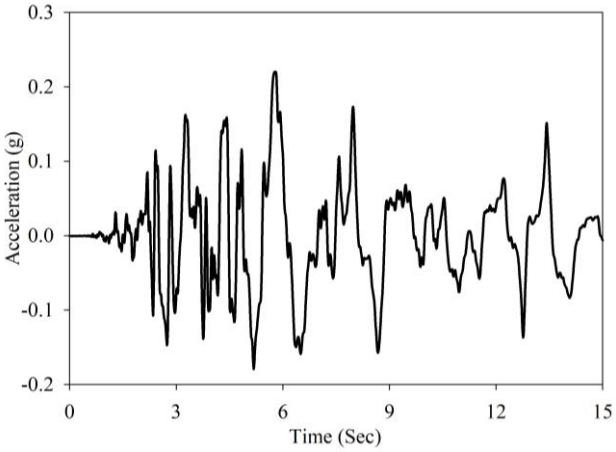

(a) Scaled Kobe earthquake

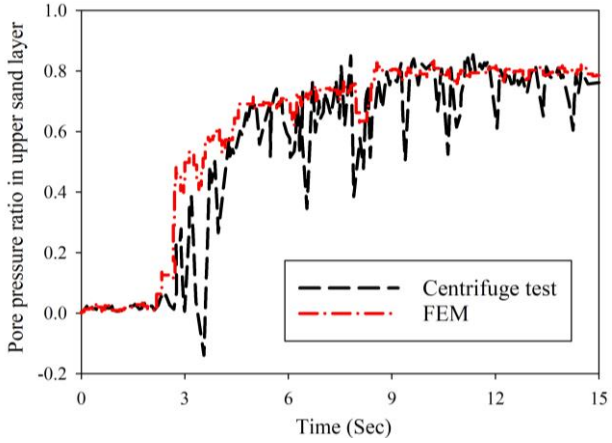

(b) Pore pressure ratio time history

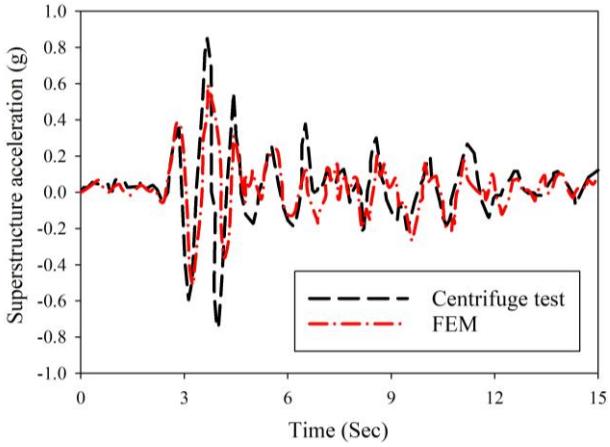

(c) Superstructure time history

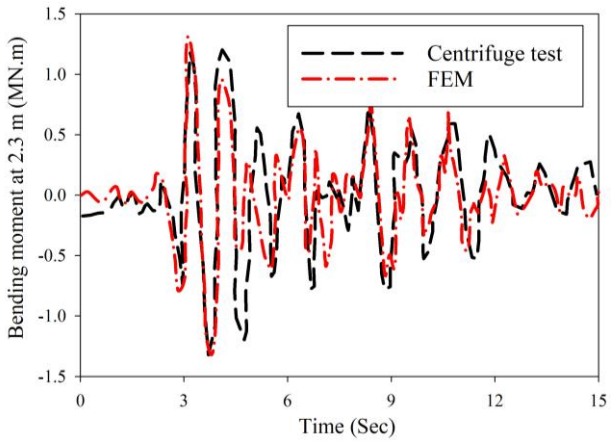

(d) Bending moment time history

Fig. 5 Comparison of the results of the FEM model with the Centrifuge test of Wilson *et al*. (1999)

subsequent increase in soil stiffness is sufficient to cause tremendous spikes in the acceleration through the ground and to the superstructure while the earthquake loading was still underway.

The dilative behavior of the soil has not been considered in the numerical model. Currently, only the generation of pore pressure caused by cyclic loading and dissipation to the soil as a result of vertical drainage can be modeled. Hence, we cannot predict the observed radical declines in pore pressure with the numerical model, but we can model the top pore pressure caused at the time of the earthquake, which generally agrees with the centrifuge test. As can be seen in the distribution of superstructure acceleration in Fig. 6, numerical results agree well with those from the centrifuge test, with one exception: the point at which pore pressure goes below zero because of soil dilation. As previously discussed, the centrifuge test sees a fall in pore pressure because of dilation, having raised the shear modulus of the soil. It follows that the superstructure acceleration in the centrifuge test exceeds that seen in the numerical model, which does not include the soil dilative behavior.

When designing a pile foundation that is subjected to earthquake loading, the criterion with the highest significance is the maximum bending moment reached. Considering the distribution of the bending moment at the depth of 2.3 m shown in Fig. 5, the top bending moment corresponds to the abrupt rise in pore pressure seen in the upper layer approximately 3.5 s after the earthquake loading application. As the current numerical model can reasonably efficiently simulate the generation of pore pressure, the top bending moment in the numerical model well agrees with that obtained in the centrifuge test. As a result, we can conclude that the dilation of the soil does not significantly impact the pile bending moment in liquefiable soil as the top bending moment caused in the pile corresponds to the soil softening that results from the rise in pore pressure. The fall in pore pressure as a result of the dilation of the soil tends to decrease the top bending moment. Soil softening due to the rise in pore pressure is evident in the bending moment and in the time-history of the acceleration as a rise in the essential period of the structure.

In Fig. 5 the FE results are given with proper mesh size (11D for the far-field region and 5D for the near-field region). The results with mesh size less than 11D for the far-field region had a difference with the centrifuge test of Wilson *et al*. (1999). Also, mesh size greater than 11D had no significant difference between the results. Therefore, to reduce the solution time of the problem, the 11D size of element was chosen.

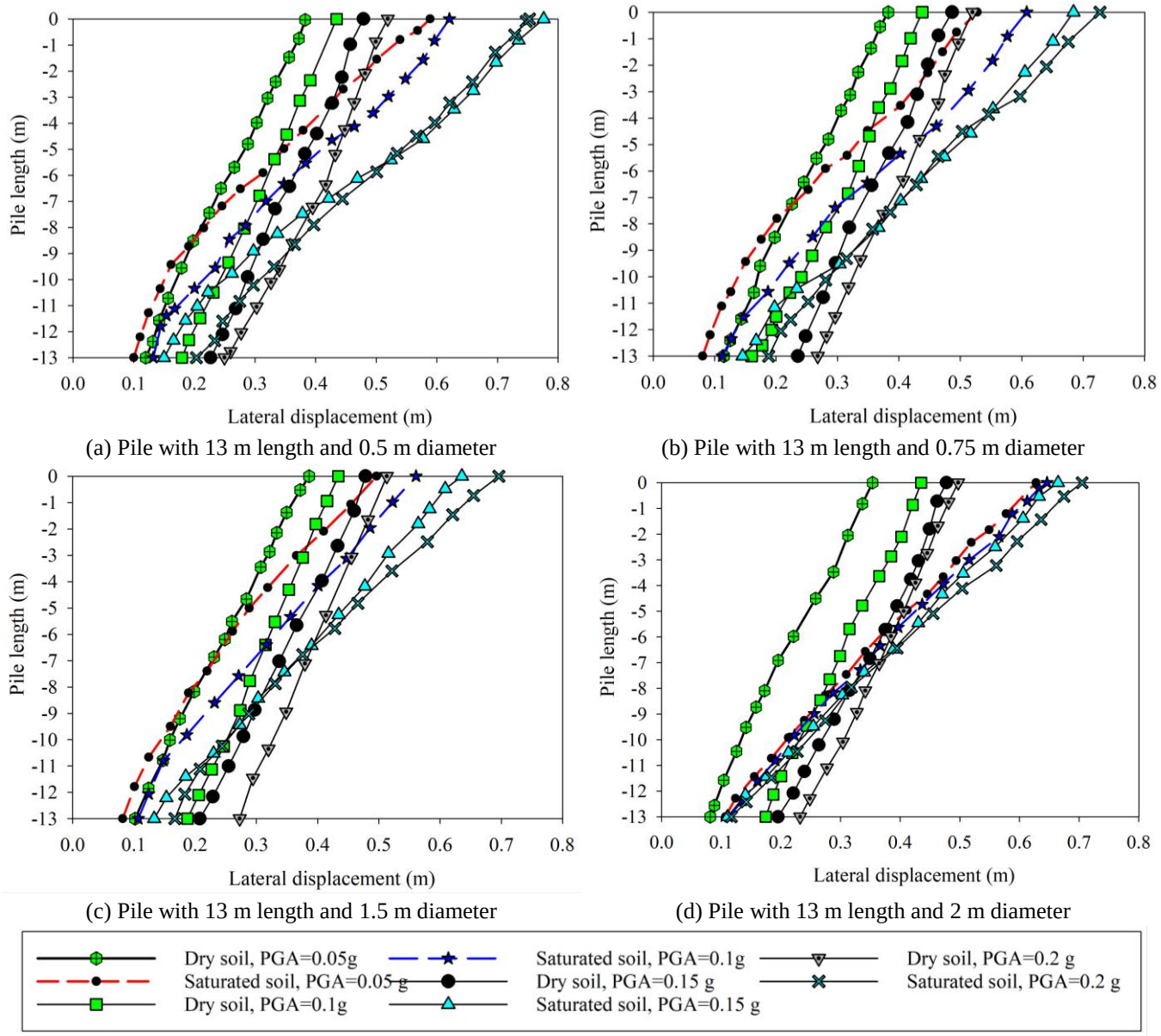

Fig. 6 Lateral displacement of pile length of 13 m under different base accelerations and diameters

4. Numerical results

To assess the influences of soil liquefaction on pile efficiency, varying geometric features of the pile and maximum earthquake acceleration were carried out in a parametric analysis.

4.1 Lateral displacement of the pile

In Fig. 6, the distribution of lateral pile deformation has been shown in the 13 m pile length under different base accelerations and in terms of two types of dry and saturated soils. It may be perceived considering that under dry state, notwithstanding the pile stiffness (i.e., diameter), the deformation of all states is linear and rotational, whilst in saturated soil state, it is observed that for piles of 0.50 and 0.75 m, the pile deformation is of flexural type. This is due to the weaker flexural rigidity of the piles, as in a pile of 1.00 m and 1.50 m diameters, the deformation is of rotational and linear type. The other matter to be pointed

Table 2. Maximum lateral displacement of the head of pile with different diameters.

Length (m)	Diameter (m)	Maximum acceleration (g) 0.05g	0.1g	0.15g	0.2g
		Maximum lateral displacement (m)			
13 m	0.50 m	0.59 m	0.62 m	0.78 m	0.75 m
	0.75 m	0.63 m	0.65 m	0.66 m	0.71 m
	1.00 m	0.50 m	0.56 m	0.64 m	0.70 m
	1.50 m	0.53 m	0.61 m	0.68 m	0.73 m
16 m	0.50 m	0.59 m	0.61 m	0.66 m	0.74 m
	0.75 m	0.71 m	0.65 m	0.63 m	0.63 m
	1.00 m	0.52 m	0.55 m	0.59 m	0.63 m
	1.50 m	0.59 m	0.55 m	0.52 m	0.50 m

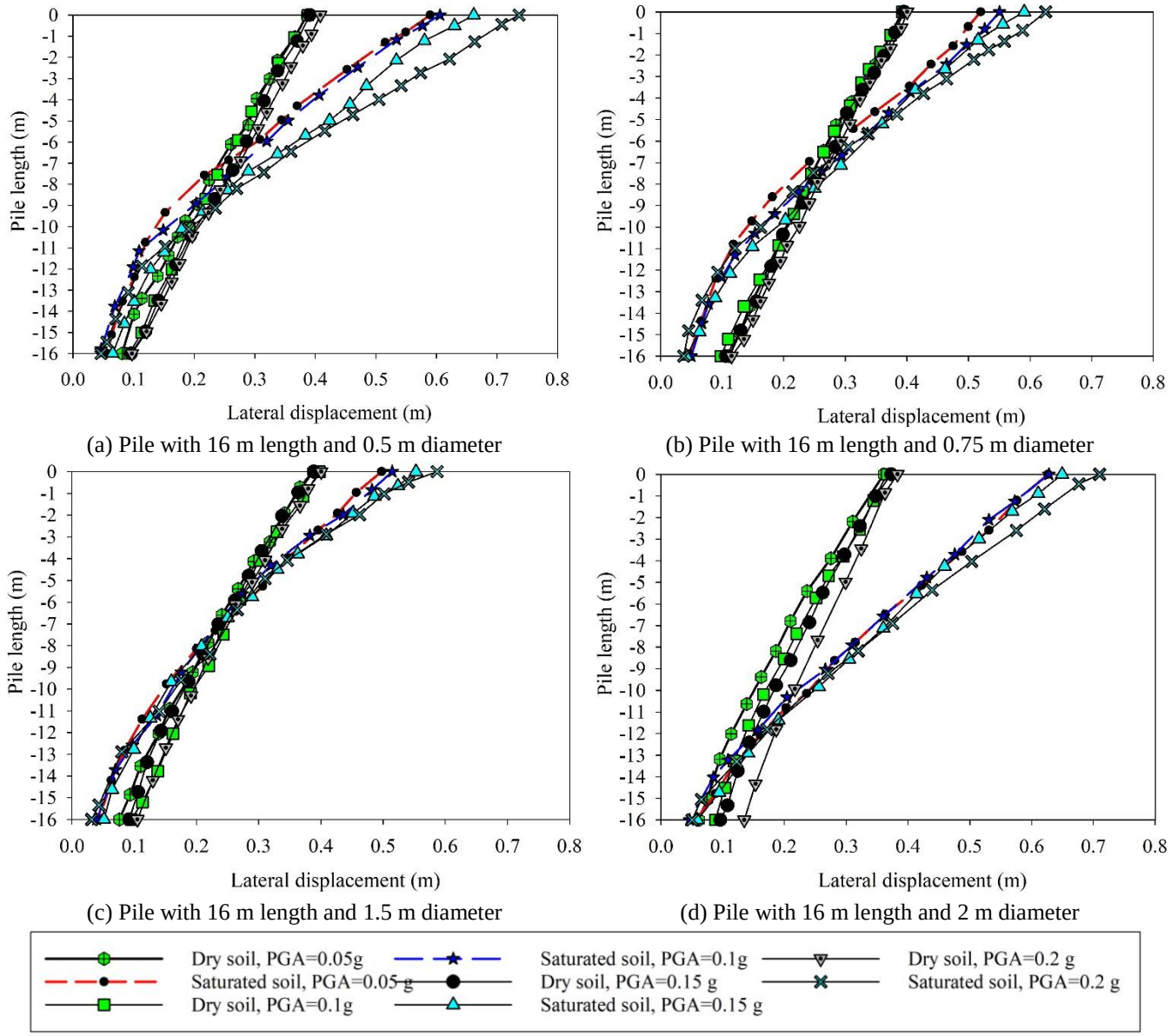

(a) Pile with 16 m length and 0.5 m diameter

(b) Pile with 16 m length and 0.75 m diameter

(c) Pile with 16 m length and 1.5 m diameter

(d) Pile with 16 m length and 2 m diameter

Fig. 7 Lateral displacement of pile length of 16 m under different base accelerations and diameters

out is that in saturated soil for smaller diameters of piles, a slight break is seen in some areas, which is due to the existence of two liquefaction layers, which is less seen for larger diameters. Meanwhile, upon increasing acceleration, pile end displacement difference in two dry and saturated states increases, in a way that in the pile of 0.50 m diameter, and 0.05g, such difference is roughly 20 cm, while the value for the same pile with 0.15g is 35 cm. However, the change to the pile end is ignorable. In Table 2, the maximum displacement of pile end under saturation has been given for different accelerations.

In Fig. 7, the distribution of lateral pile deformation has been shown in the 16m pile length under different base accelerations and in terms of two types of dry and saturated soils. It may be perceived considering that under dry state, notwithstanding the pile stiffness (i.e., diameter), the deformation of all states is linear and rotational, while in saturated soil state, it is observed that for piles of 0.50 and 0.75 m, the pile deformation is of bending type. This is due to the weaker bending rigidity of the piles, as in the pile of 1.0 m and 1.5 m diameters, the deformation is of rotational and linear type. All the facts on 13 m piles are true to 16 m piles. However, it is seen that by increasing the length from 13 m to 16 m, the deformations are not changing, and also displacement at the buried end of the pile is low. By increasing acceleration, pile end displacement difference in two dry and saturated states increases, in a way that in a pile diameter of 0.50 m, and under a base acceleration of 0.05g, such difference is roughly 200 mm, while the value for the same pile with 0.15g is 260 mm. In Table 2, the maximum displacement of pile end under saturation has been given for different accelerations.

4.2 Base acceleration on pile response

In Fig. 8, the 13 m pile length displacement changes have been shown considering the quake base acceleration

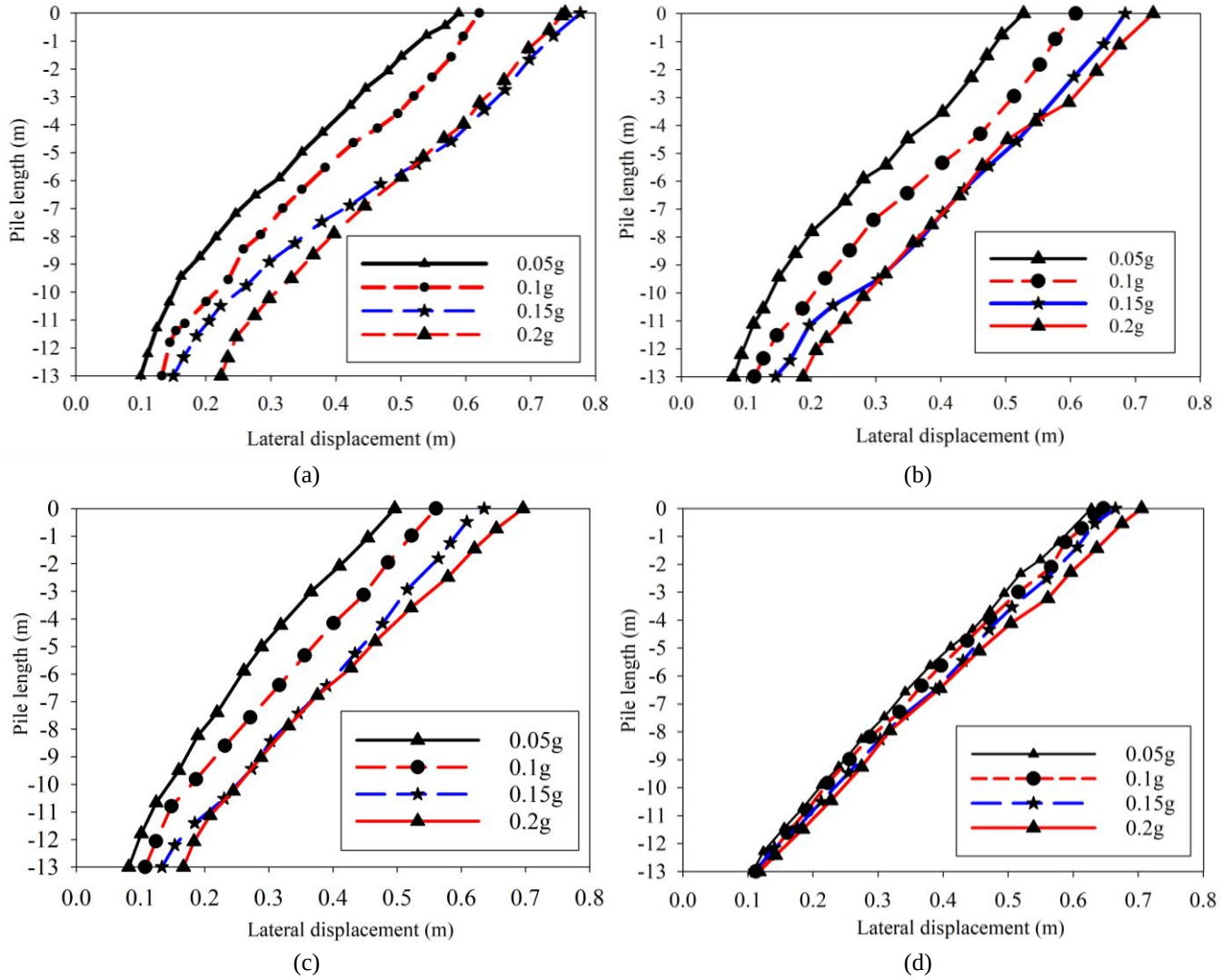

Fig. 8 Lateral displacement of the pile with length of 13 m under different base accelerations for various diameters (a) 0.50 m, (b) 0.75 m, (c) 1.00 m, and (d) 1.50 m

changes. As it may be seen, by increasing acceleration and with a fixed diameter, the pile displacement increases. For instance, regarding a 50 cm diameter pile, such growth reaches from 58 cm to 77 cm, while by increasing diameter, such growth reaches 13%. In other words, by increasing the diameter, the displacement difference also decreases. On the other hand, the relative displacement of two ends of the pile also highly decreases.

In Fig. 9, the deformation changes in terms of diameter have been shown. Considering Fig. 9, by increasing diameter in all states (except for 50 cm diameter), the displacements increased upon 0.15g. Meanwhile, by increasing diameter from 100 cm to 150 cm, no big change was seen in the pile end displacement decrease. In other words, also for bigger acceleration pile of 100 cm diameter may be used instead of a pile of 150 cm in diameter. However, it is probably for the higher accelerations, and considering real structure weight, the concrete pile rigidity with 100 cm diameter is not sufficient and breaks the pile in the liquefied soil spot. Therefore, regarding implementation and realistic considerations, the 150 cm diameter of the pile is more suitable in terms of bending rigidity.

It may be concluded that pile lateral displacement is subject to maximum acceleration. Also pile diameter highly influence pile deformation, which is seen in small and average diameter piles. On the other hand, regarding piles of diameters bigger than 1.00 m, the diameter effect on reducing pile displacement decreases. Therefore, a 1.00 m pile diameter may be a more cost-effective option.

4.3 Distribution of bending moment along with the pile

It may be seen considering Fig. 10 for different diameters of a fixed length of 13m that increasing diameter shall further increase flexural rigidity and generates higher flexural needs. In 0.05g base acceleration, the increase in bending moment reaches with 50cm diameter of the pile to 1.50 m diameter from 258 kN to 984 kN, i.e., 8.2 times bigger. A gradual increase in base acceleration to 0.2g causes such growth to reach 120%. Meanwhile, the highest value of bending moment has occurred in the layer between

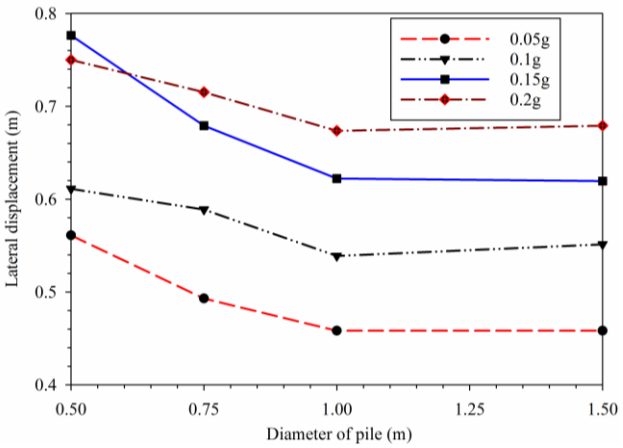

Fig. 9 Changes of lateral displacement for different diameters under different peak accelerations

two liquefiable layers, which is of better compaction, and also soil resisting pressure to pile increases. Therefore, the bending moment and diameter of the pile are directly relevant, as shown in Fig. 11.

Considering Fig. 12 for different diameters of the pile and 16 m length, it is seen that increasing diameter shall further increase flexural rigidity and generates higher flexural demand. The bending moment changes along the pile is like that of 13 m length of the pile. In 0.05g base acceleration, the increase in bending moment reaches with a diameter of 0.50 m pile to 1.50 m diameter from 273 kN to 990 kN, i.e., 6.2 times bigger. A gradual increase in base acceleration to 0.2g causes such growth to reach 54%. Meanwhile, it is seen that the maximum bending moment has occurred in the layer between two liquefiable layers, which is of better compaction, and also soil resisting pressure to pile increases.

4.4 Pore pressure development on pile behavior

Even though numerical methods are designed to acquire the performance of the pile while subjected to earthquake loading, a large number of them do not incorporate the influence of soil strength and stiffness degradation caused by the generation of pore pressure and by the following soil liquefaction (Kavvadas and Gazetas 1993, Norris 1994, El Naggar and Novak 1996, Tabesh and Poulos 2001). In many cases, hence, the pile is designed according to the top bending moments and shear forces computed on the assumption that soil is a linear elastic material or a nonlinear material, and not taking into account strength and stiffness degradation caused by the generation of pore pressure. Thus, here the results from the effective stress analysis, previously described, are compared with a total stress analysis without considering any pore pressure effects, while including the soil nonlinear behavior.

Before discussing pile behavior in detail, we must study the effect of the generation of pore pressure on ground motion, which decides the pile's kinematic bending. In Fig. 13, we can see the ratio of the effective over the total maximum ground displacement, occurring at the ground surface, acquired from both effective and total analyses. In

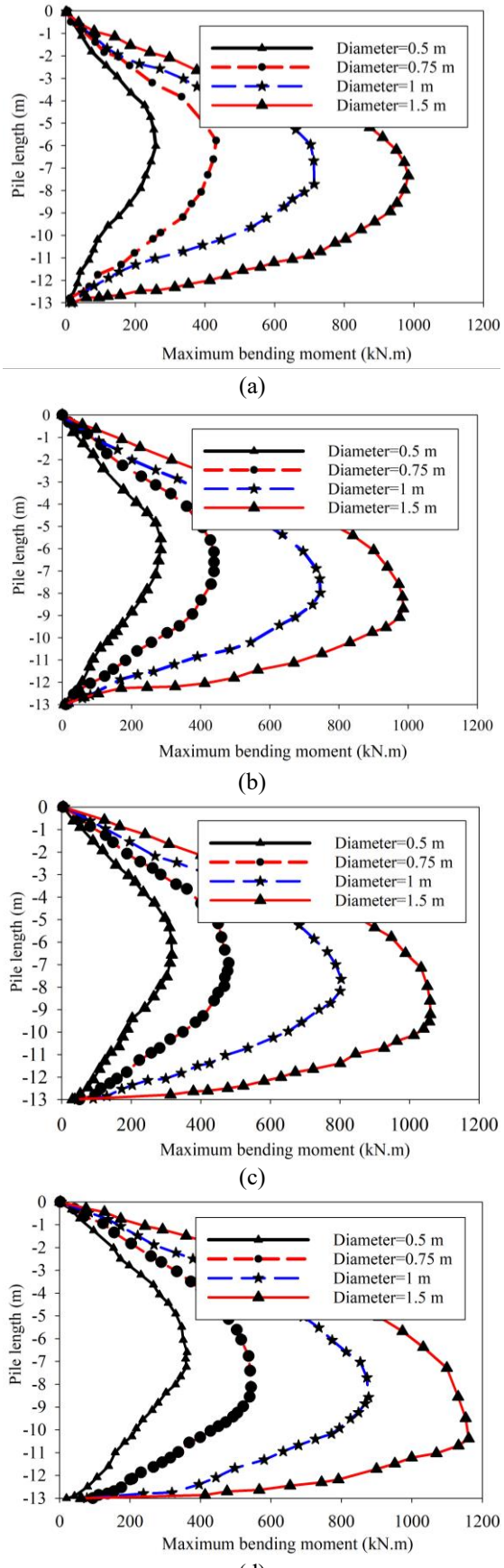

Fig. 10 Bending moment distribution along the piles with length of 13 m for various diameters under different peak accelerations (a) 0.05g, (b) 0.1g, (c) 0.15g, and (d) 0.2g

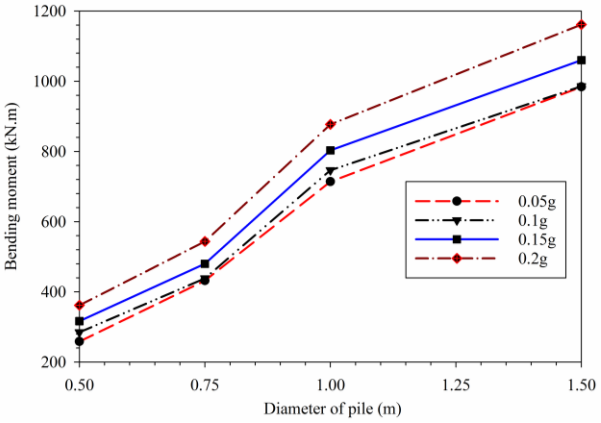

Fig. 11 Relationship between bending moment and pile diameter for a length of 13 m under different peak accelerations

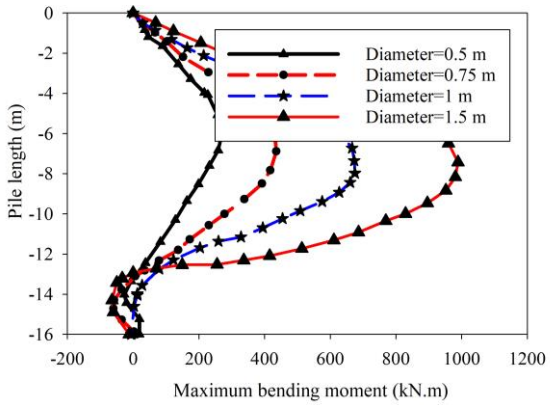

(a)

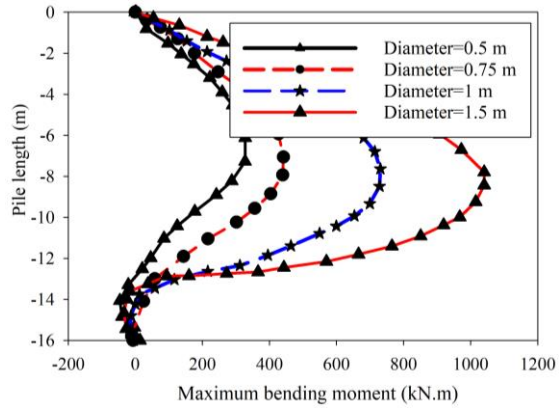

(b)

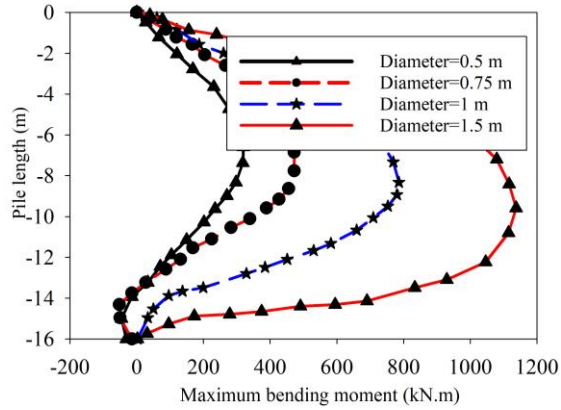

(c)

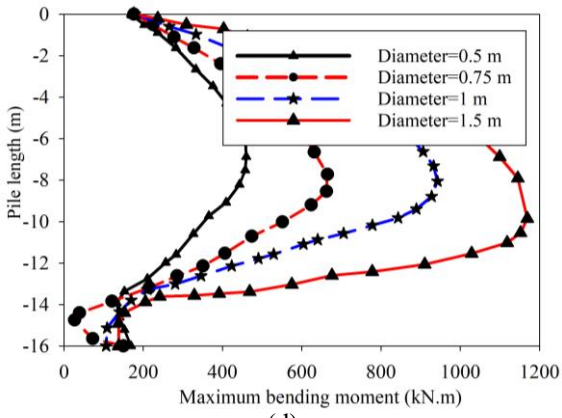

(d)

Fig. 12 Bending moment distribution along the piles with length of 16 m and various diameters and peak accelerations (a) 0.05g, (b) 0.1g, (c) 0.15g, and (d) 0.2g

certain instances, it can be shown that the maximum ground displacement obtained from the effective stress analysis is over four times as much as that obtained from the overall stress analysis.

The ratio of the effective and total stress analyses for the highest amount of bending moment, relative displacement, acceleration of the pile head, and shear load can be seen in Fig. 14.

Piles that carry cap masses have been employed for the analysis to take into account the superstructure load which is transferred to the piles. Including the generation of pore pressure, in every single case, has raised the highest bending moment and the deformation occurring at the pile head. The maximum acceleration of pile heads has fallen, in many cases, when the impact of pore pressure is incorporated. This is caused by the soil softening; namely, soil softening will raise the lateral ground displacements working upon the pile, which makes the peaks and troughs of high frequency in the acceleration of the pile head smoother. Accordingly, we can conclude that when incorporating the pore pressure generation, the bending caused by kinematic forces is more significant than that caused by inertia forces.

The highest value of pile bending moment occurs at the head of the pile. However, the highest amount of shear load in Fig. 14(d) does not occur there in every case. Yet, it develops in the highest 25% of the length of the pile. Upon careful examination of Fig. 15(d), we can see that in certain cases, the incorporation of the generation of pore pressure raises the top shear load that occurs in the pile, whereas in other cases, it decreases the top shear force.

If the top shear force occurs at the pile head, the inertia force there (cap-mass x pile head acceleration) decides the shear force. As a result, when the pore pressure impact is incorporated, the maximum shear force declines. In other instances, kinematic forces caused by huge soil displacements (due to pore pressure generation and the following soil softening) are of a more significant impact than the pile head inertia force. Hence, when incorporating pore pressure development, the top shear force in the pile rises.

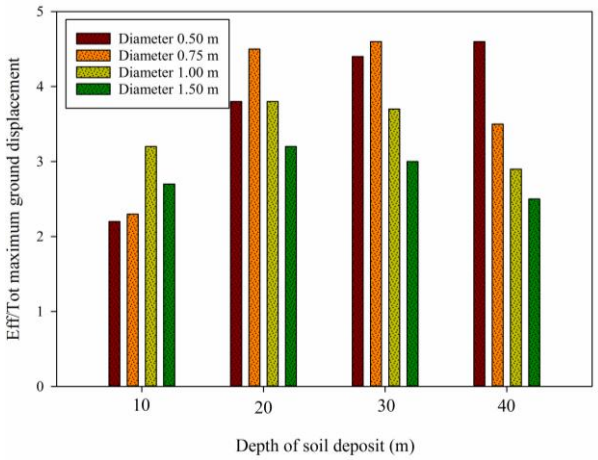

Fig. 13 Comparison of maximum ground displacement obtained from effective and total stress analyses

When conducting total stress analysis, despite ignoring the generation of pore pressure, soil softening will develop as a result of soil yielding. As a result, in the lack of liquefaction, the highest value of shear strength and bending moment from effective and total stress analyzes correlate practically. Figs. 14(a,d) show this when the soil's relative density is 90%. As a result, in the absence of liquefaction, top bending moment and shear force occurring in a pile can be acquired from a total stress analysis, incorporating the soil's nonlinear behavior. Nonetheless, in the presence of liquefaction, we should conduct an effective stress-based ground response analysis to find the top bending moment and shear force occurring in the pile.

5. Conclusions

In this study, the finite element method has been used to simulate the pile behavior in liquefiable soil. The parameters affecting the pile response, such as diameter, pile length, soil type, and base acceleration, were investigated. A number of 3D FE models were suggested to study the system behavior. The soil was exposed to liquefaction in two layers. During this study, the pile was modeled as a 1D element, while its surrounding soils were modeled as continuous brick elements. Totally 64 non-linear time-history analyses were conducted. The pile's deformation responses in the depth of soil, bending moment in a pile were studied, and the relation between such parameters, as well as the effect of pore pressure on pile performance, were investigated. The summary of the findings follows:

- The lateral deformations of the pile have slightly intensified due to soil considering two liquefiable layers. Such issues are seen in both the dry and the saturated states.
- The displacement of the top part of the pile in the saturated state is larger than in the dry state, which is due to sand soil layer liquefaction in the two layers of 5 m and 11 m depths.
- A pile diameter smaller than 0.75 m is more tended to have flexural behavior like a cantilever beam. In other

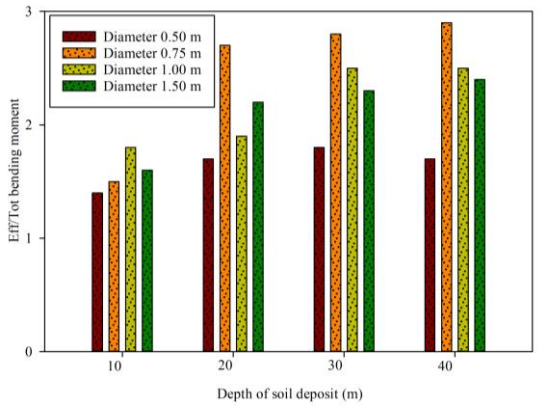

(a) Bending moment ratio

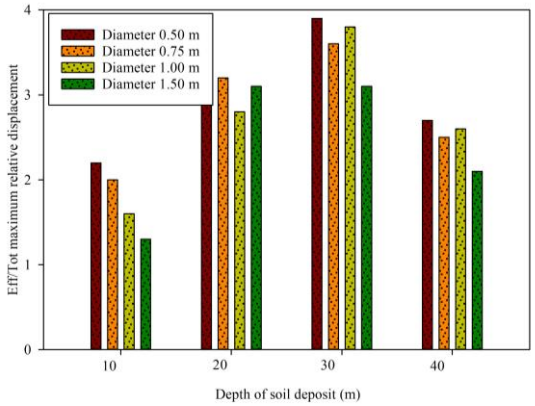

(b) Relative displacement

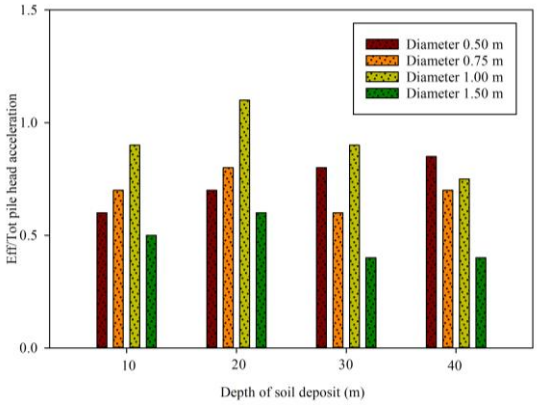

(c) Pile head acceleration ratio

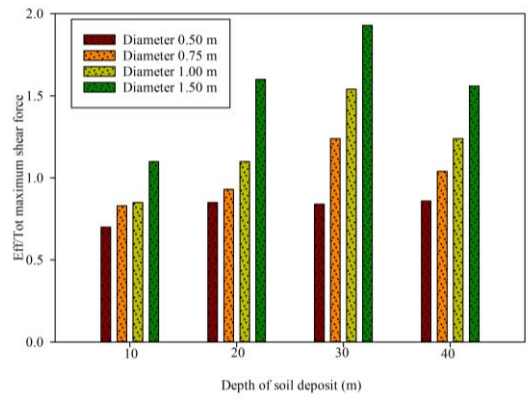

(d) Maximum shear force ratio

Fig. 14 Comparison of results obtained from the effective stress and total stress analyses

words, larger pile diameters rotate rigidly due to higher flexural rigidity.

- Among the studied parameters, the pile diameter has the biggest effect on the pile-soil system behavior. Meanwhile, in this study, using a pile diameter of 1.50 m has not decreased the pile displacement in comparison to the 1.00 m pile diameter. Therefore, using the latter is suggested, due to being more cost-effective.
- The pile lateral displacement is directly associated with the maximum acceleration, while such relation is slightly non-linear.
- The bending moment model for the 13 m length of the pile is similar to cantilever beams, while for the 16 m length of pile, it is slightly changed at the pile end.
- Increasing pile diameter increases the flexural rigidity, eventually due to the increased contact surface with the soil. It increases resisting soil pressure.
- Low base accelerations may not release enough energy to fully form liquefaction phenomena. Therefore, in higher base accelerations, the pile displacement increases, and it indicates that there is no lateral shear strength from the liquefiable layer of the soil.
- An effective stress-ground response analysis should be performed when there is a liquefiable layer to determine the maximum bending moment and shear load developed in the pile.
- One of the limitations of this study is that the seismic behavior of the superstructure is not considered. This is due to the nonlinear complexity of the material behavior. Another limitation is the time-consuming analysis for pile groups. In this case, other researchers consider the continuity/detachment of the foundation to the superstructure (e.g., bridge and structural buildings). For future work, it is suggested that the structural frames above the foundation should be considered and also investigate other foundation types like caisson and pile-foundation with base isolators.

References

ABAQUS, Version 6.14 (2014), Documentation, Dassault Systemes Simulia Corporation; Providence, RI, USA. http://130.149.89.49:2080/v6.14.

Abate, G., Caruso, C., Massimino, M.R. and Maugeri, M. (2008), "Evaluation of shallow foundation settlements by an elasto-plastic kinematic-isotropic hardening numerical model for granular soil", *Geomech. Geoeng.*, **3**(1), 27-40. https://doi.org/10.1080/17486020701862174.

Abdoun, T. and Dobry, R. (2002), "Evaluation of pile foundation response to lateral spreading", *Soil Dynam. Earthq. Eng.*, **22**(9-12), 1051-1058. https://doi.org/10.1016/S0267-7261(02)00130-6.

Abdoun, T., Dobry, R., and O'Rouke, T.D. (1997), "Centrifuge and numerical modeling of soil-pile interaction during earthquake induced soil liquefaction and lateral spreading", *Geotech. Special Publication*, **64**, 76-82.

Bagheri, M., Ebadi-Jamkhaneh, M. and Samali, B. (2018), "Effect of seismic soil–pile–structure interaction on mid- and high-rise steel buildings resting on a group of pile foundations", *J. Geomech.*, **18**(9), 04018103. https://doi.org/10.1061/(ASCE)GM.1943-5622.0001222

Bahrami, M., Khodakarami, M.I. and Kontoni, D.-P.N. (2015), "Analysis of the dynamic soil-pile interaction during the passage of Rayleigh waves using Fourier transform", *Proceedings of the 6th International Conference on Experiments/ Process/ System Modeling/ Simulation/ Optimization (6th IC-EpsMsO)*, Athens, July.

Been, K. and Jefferies, M.G. (1985), "A state parameter for sands", *Geotechnique*, **35**(1), 99-112. https://doi.org/10.1680/geot.1985.35.2.99.

Canou, J., Bahloul, A., Attar, A. and Piffer, L. (1992), "Evaluation of a liquefaction criterion of a loose sand", *Proceedings of the 10th World Conference on Earthquake Engineering*, **3**, 1367-1372, Madrid, July.

Chang, G.S. and Kutter, B.L. (1989), "Centrifugal modeling of soil-pile-structure interaction", *Engineering Geology and Geotechnical Engineering: Proceedings of the 25th Symposium*, 327-336, A.A. Balkema, Netherlands.

Cheng, Z. and Jeremic, B. (2009), "Numerical modeling and simulation of pile in liquefiable soil", *Soil Dynam. Earthq. Eng.*, **29**(11-12), 1405-1416. https://doi.org/10.1016/j.soildyn.2009.02.008

Chong, S.H., Shin, H.S. and Cho, G.C. (2019), "Numerical analysis of offshore monopile during repetitive lateral loading", *Geomech. Eng.*, **19**(1), 79-91. http://dx.doi.org/10.12989/gae.2019.19.1.079.

Comodromos, E.M., Papadopoulou, M.C. and Rentzepris, I.K. (2009), "Pile foundation analysis and design using experimental data and 3-D numerical analysis", *Comput. Geotech.*, **36**(5), 819-836. https://doi.org/10.1016/j.compgeo.2009.01.011

Cui, C.Y., Meng, K., Wu, Y.J., Chapman, D. and Liang, Z.M. (2018), "Dynamic response of pipe pile embedded in layered visco-elastic media with radial inhomogeneity under vertical excitation", *Geomech. Eng.*, **16**(6), 609-618. http://dx.doi.org/10.12989/gae.2018.16.6.609

Dobry, R., Taboada, V. and Liu, L. (1995), "Centrifuge modeling of liquefaction effects during earthquakes", *Proceedings of the First Conference on Earthquake Geotechnical Engineering*, 1291-1324, A.A. Balkema, Netherlands.

Ebeido, A., Elgamal, A., Tokimatsu, K. and Abe, A. (2019), "Pile and pile-group response to liquefaction-induced lateral spreading in four large-scale shake-table experiments", *J. Geotech. Geoenviron. Eng.*, **145**(10), 04019080. https://doi.org/10.1061/(ASCE)GT.1943-5606.0002142.

El Naggar, M.H. and Novak, M. (1996), "Non-linear analysis for dynamic lateral pile response", *Soil Dynam. Earthq. Eng.*, **15**(4), 233-244. https://doi.org/10.1016/0267-7261(95)00049-6

Farghaly, A.A. and Kontoni, D.-P.N. (2018), "Nonlinear analysis of a riverine platform under earthquake and environmental loads", *Wind Struct.*, **26**(6), 343-354. https://doi.org/10.12989/was.2018.26.6.343

Finn, W.D.L. and Gohl, W.B. (1987), "Centrifuge model studies of piles under simulated earthquake loading from dynamic response of pile foundations-experiment, analysis, and observation", *Geotech. Special Publication*, **11**, 21-38.

Finn, W.D.L. and Fujita, N. (2002), "Piles in liquefiable soils: seismic analysis and design issues", *Soil Dynam. Earthq. Eng.*, **22**(9-12), 731-742. https://doi.org/10.1016/S0267-7261(02)00094-5.

Gajo, A. and Wood, M. (1999), "Severn-Trent sand: A kinematic hardening constitutive model: The q-p formulation", *Geotechnique*, **49**(5), 595-614. https://doi.org/10.1680/geot.1999.49.5.595.

Haeri, S.M., Kavand, A., Rahmani, I. and Torabi, H. (2012), "Response of a group of piles to liquefaction-induced lateral spreading by large scale shake table testing", *Soil Dynam. Earthq. Eng.*, **38**, 25-45. https://doi.org/10.1016/j.soildyn.2012.02.002

Han, J.T., Kim, S.R., Hwang, J.I. and Kim, M.M. (2007), "Evaluation of the dynamic characteristics of soil-pile system in

liquefiable ground by shaking table tests", *The 4th International Conference on Earthquake Geotechnical Engineering*, Thessaloniki, June.

Horikoshi, K., Tateishi, A. and Fujiwara, T. (1998), "Centrifuge modeling of a single pile subjected to liquefaction-induced lateral spreading", *Soils Foundations*, **38**, 193-208. https://doi.org/10.3208/sandf.38.Special_193

Hushmand, B., Scott, R.F. and Crouse, C.B. (1998), "Centrifuge liquefaction tests in a laminar box", *Geotechnique*, **38**(2), 253-262. https://doi.org/10.1680/geot.1988.38.2.253

Hussein, A.F. and El Naggar, M.H. (2021), "Seismic axial behaviour of pile groups in non-liquefiable and liquefiable soils", *Soil Dynam. Earthq. Eng.*, **149**, 106853. https://doi.org/10.1016/j.soildyn.2021.106853.

Jiang, S., Du, C. and Sun, L. (2018), "Numerical analysis of sheet pile wall structure considering soil-structure interaction", *Geomech. Eng.*, **16**(3), 309-320. http://dx.doi.org/10.12989/gae.2018.16.3.309.

Jiménez, G.A.L., Dias, D. and Jenck, O. (2019), "Effect of layered liquefiable deposits on the seismic response of soil-foundations-structure systems", *Soil Dynam. Earthq. Eng.*, **124**, 1-15. https://doi.org/10.1016/j.soildyn.2019.05.026.

Kavvadas, M. and Gazetas, G. (1993), "Kinematic seismic response and bending of free-head piles in layered soils", *Geotechnique*, **43**(2), 207-222. https://doi.org/10.1680/geot.1993.43.2.207.

Khakpour Moghaddam, H., Khodakarami, M.I. and Kontoni, D.-P.N. (2015), "Assessment of the under-ground water level effects on the nonlinear behavior of single pile subjected to static vertical loads in the presence of soil-pile interaction", *Proceedings of the 8th GRACM International Congress on Computational Mechanics (8th GRACM)*, University of Thessaly Press, Volos, Greece.

Kheradi, H., Morikawa, Y., Ye, G. and Zhang, F. (2019), "Liquefaction-induced buckling failure of group-pile foundation and countermeasure by partial ground improvement", *J. Geomech.*, **19**(5), 04019020. https://doi.org/10.1061/(ASCE)GM.1943-5622.0001379

Kim, Y.S. and Choi, J.I. (2017), "Nonlinear numerical analyses of a pile-soil system under sinusoidal bedrock loadings verifying centrifuge model test results", *Geomech. Eng.*, **12**(2), 239-255. http://dx.doi.org/10.12989/gae.2017.12.2.239

Klar, A., Baker, R. and Frydman, S. (2004), "Seismic soil-pile interaction in liquefiable soil", *Soil Dynam. Earthq. Eng.*, **24**(8), 551-564. https://doi.org/10.1016/j.soildyn.2003.10.006.

Kontoni, D.-P.N. and Farghaly, A.A. (2018), "3D FEM analysis of a pile-supported riverine platform under environmental loads incorporating soil-pile interaction", *Computation*, **6**(1), 8. https://doi.org/10.3390/computation6010008.

Liu, L. and Dobry, R. (1995), "Effect of liquefaction on lateral response of piles by centrifuge model tests", *NCEER Bulletin*, **9**(1), 7-11. https://rosap.ntl.bts.gov/view/dot/13895.

Mizuno, H. and Liba, M. (1982), "Shaking table testing of seismic building-pile-soil interaction", *Proceedings of the 5th Japan Earthquake Engineering Symposium*, Tokyo, Japan, 1713-1720.

Mizuno, H., Sugimoto, M., Mori, T., Iiba, M. and Hirade, T. (2000), "Dynamic behavior of pile foundation in liquefaction process- Shaking table tests utilizing big shear box", *Proceedings of the 12th World Conference on Earthquake Engineering*, Auckland, January.

Nakamura, T., Sugano, T., Oikawa, K. and Mito, M. (2000), "An experimental study on the pier damaged by 1995 Hyogoken-Nanbu earthquake", *Proceedings of the 12th World Conference on Earthquake Engineering*, Auckland, January.

Norris, G. M. (1994), "Seismic bridge pile foundation behavior", *Proceedings of the International Conference on Design and Construction of Deep Foundations*, **1**, 27-136.

Ohtomo, K. (1996), "Effects of liquefaction induced lateral flow on a conduit with supporting piles", *Proceedings of the 11th World Conference on Earthquake Engineering*, Acapulco, June.

Oka, F., Lu, C.W., Uzuoka, R. and Zhang, F. (2004), "Numerical study of structure-soil-group pile foundations using an effective stress based liquefaction analysis method", *Proceedings of the 13th World Conference on Earthquake Engineering*, Vancouver, August.

Peck, R.B., Hanson, W.E. and Thornburn, T.H. (1974), *Foundation Engineering*, 2nd Ed., John Wiley and Sons, NJ, USA.

PEER (2012), PEER ground motion database; Pacific Earthquake Engineering Research Center, University of California, Berkeley, USA.

Rahmani, A. and Pak, A. (2012), "Dynamic behavior of pile foundations under cyclic loading in liquefiable soils" *Comput. Geotech.*, **40**, 114-126. https://doi.org/10.1016/j.compgeo.2011.09.002

Su, D. and Li, X.S. (2006), "Effect of shaking intensity on seismic response of single-pile foundation in liquefiable soil", *Proceedings of the Ground Modification and Seismic Mitigation*, *GeoShanghai International Conference*, Shanghai, June. 379-386. https://doi.org/10.1061/40864(196)51

Tabesh, A. and Poulos, H. G. (2001), "The effect of soil yielding on seismic response of single piles", *Soils Foundations*, **41**(3), 1-16. https://doi.org/10.3208/sandf.41.3_1

Tajirian, F.F., Tabatabaie, M. and Rao, P. (2019), "Soil-Structure interaction analysis of a large diameter tank on piled foundations in liquefiable soil", *Geo-Congress 2019: Earthquake Engineering and Soil Dynamics*, 169-180. American Society of Civil Engineers, Reston, USA. https://doi.org/10.1061/9780784482100.018.

Tamura, S. and Tokimatsu, K. (2005), "Seismic earth pressure acting on embedded footing based on large-scale shaking table tests", *Proceedings of the Workshop on Seismic Performance and Simulation of Pile Foundations in Liquefied and Laterally Spreading Ground*, University of California, 83-96. https://doi.org/10.1061/40822(184)8

Tamura, S., Suzuki, Y., Tsuchiya, T., Fujii, S. and Kagawa, T. (2000), "Dynamic response and failure mechanisms of a pile foundation during soil liquefaction by shaking table test with a large scale laminar shear box", *Proceedings of the 12th World Conference on Earthquake Engineering*, Auckland, Auckland, January.

Tatsuoka, F. and Ishihara, K. (1974), "Drained deformation of sand under cyclic stresses reversing direction", *Soils Foundations*, **14**(3), 51-65. https://doi.org/10.3208/sandf1972.14.3_51.

Towhata, I. (2008), *Geotechnical Earthquake Engineering*, Springer-Verlag, Berlin-Heidelberg, Germany.

Trochanis, A., Bielak, J. and Christiano, P. (1991), "Simplified model for analysis of one or two piles", *J. Geotech. Eng.*, **117**(3), 448-466. https://doi.org/10.1061/(ASCE)0733-9410(1991)117:3(448).

Uzuoka, R., Sento, N., Kazama, M., Zhang, F., Yashima, A. and Oka, F. (2007), "Three-dimensional numerical simulation of earthquake damage to group-piles in a liquefied ground", *Soil Dynam. Earthq. Eng.*, **27**(5), 395-413. https://doi.org/10.1016/j.soildyn.2006.10.003.

Watcharasawe, K., Jongpradist, P., Kitiyodom, P., and Matsumoto, T. (2021), "Measurements and analysis of load sharing between piles and raft in a pile foundation in clay", *Geomech. Eng.*, **24**(6), 559-572. http://dx.doi.org/10.12989/gae.2021.24.6.559.

Wilson, D.W. (1998), "Soil-pile-superstructure interaction in liquefying sand and soft clay", Ph.D. Dissertation, University of California, Davis.

Wilson, D.W., Boulanger, R.W. and Kutter, B.L. (1999), "Lateral resistance of piles in liquefying sand", *Proceedings of the OTRC '99 Conference on Analysis, Design, Construction, and Testing*

of Deep Foundations, *Geotech. Special Publication*, **88**, 165-179.

Wilson, D.W., Boulanger, R.W. and Kutter, B.L. (2000), "Observed seismic lateral resistance of liquefying sand", *J. Geotech. Geoenviron. Eng.*, **126**(10), 898-906. https://doi.org/10.1061/(ASCE)1090-0241(2000)126:10(898).

Yao, S., Kobayashi, K., Yoshida, N. and Matsuo, H. (2004), "Interactive behavior of soil-pile superstructure system in transient state to liquefaction by means of large shake table tests", *Soil Dynam. Earthq. Eng.*, **24**(5), 397-409. https://doi.org/10.1016/j.soildyn.2003.12.003.

Yasuda, S., Ishihara, K., Morimoto, I., Orense, R., Ikeda, M. and Tamura, S. (2000), "Large-scale shaking table tests on pile foundations in liquefied ground", *Proceedings of the 12th World Conference on Earthquake Engineering*, Auckland, January.

Zhang, X., Tang, L., Ling, X., Chan, A. and Jinchi, L. (2018), "Using peak ground velocity to characterize the response of soil-pile system in liquefying ground", *Eng. Geology*, **240**, 62-73. https://doi.org/10.1016/j.enggeo.2018.04.011.

Zhang, X., Tang, L., Li, X., Ling, X. and Chan, A. (2020), "Effect of the combined action of lateral load and axial load on the pile instability in liquefiable soils", *Eng. Struct.*, **205**, 110074. https://doi.org/10.1016/j.engstruct.2019.110074.

Zou, J.F., Yang, T. and Deng, D.P. (2019), "Field test of the long-term settlement for the post-grouted pile in the deep-thick soft soil", *Geomech. Eng.*, **19**(2), 115-126. http://dx.doi.org/10.12989/gae.2019.19.2.115.

CC